

Inelastic charged current interaction of supernova neutrinos in two-phase liquid xenon dark matter detectors

Pijushpani Bhattacharjee,^{1,*} Abhijit Bandyopadhyay,^{2,†} Sovan Chakraborty,^{3,‡} Sayan Ghosh,^{1,§} Kamales Kar,^{2,¶} and Satyajit Saha^{1,**}

¹*Saha Institute of Nuclear Physics, HBNI, 1/AF Bidhannagar, Kolkata 700064, India*

²*Ramakrishna Mission Vivekananda Educational and Research Institute, Belur Math, Howrah 711202, India*

³*Department of Physics, Indian Institute of Technology - Guwahati, Guwahati 781039, India*

It has been known that neutrinos from supernova (SN) bursts can give rise to nuclear recoil (NR) signals arising from coherent elastic neutrino-nucleus scattering (CE ν NS) interaction, a neutral current (NC) process, of the neutrinos with xenon nuclei in future large (multi-ton scale) liquid xenon (LXe) detectors employed for dark matter search, depending on the SN progenitor mass and distance to the SN. In this paper, we show that the same detectors will also be sensitive to inelastic charged current (CC) interactions of the SN electron neutrinos (ν_e CC) with the xenon nuclei. Such interactions, while creating an electron in the final state, also leave the post-interaction target nucleus in an excited state, the subsequent deexcitation of which produces, among other particles, gamma rays and neutrons. The electron and deexcitation gamma rays will give “electron recoil” (ER) type signals, while the deexcitation neutrons—the so called “neutrino induced neutrons” (ν_e In)—produce, through their multiple scattering on the xenon nuclei, further xenon nuclear recoils that will also give NR signals (in addition to those produced through the CE ν NS interactions). We discuss the observable scintillation and ionization signals associated with SN neutrino induced CE ν NS and ν_e CC events in a generic LXe detector and argue that upcoming sufficiently large LXe detectors should be able to detect both these types of events due to neutrinos from reasonably close by SN bursts. We also note that since the total CC induced ER and NR signals receive contributions predominantly from ν_e CC interactions while the CE ν NS contribution comes from NC interactions of *all the six species of neutrinos*, identification of the ν_e CC and CE ν NS origin events may offer the possibility of extracting useful information about the distribution of the total SN explosion energy going into different neutrino flavors.

I. INTRODUCTION

Core collapse supernova (CCSN) explosions [1] give out huge flux of neutrinos (and antineutrinos) of all flavors [2–4] with energies up to a few tens of MeV over a time scale of ~ 10 seconds. These neutrinos carry almost all ($\sim 99\%$) of the gravitational energy ($\sim 10^{53}$ erg) released due to collapse of the core of the massive progenitor star. A number of large experimental facilities around the world [5] should be able to detect the neutrinos from the next nearby (hopefully Galactic) CCSN, after the historic first detection of neutrinos from the supernova SN1987A located in the Large Magellanic Cloud (LMC) at a distance of ~ 50 kpc from Earth [6]. Detection of supernova neutrinos of different flavors from a single supernova by multiple detectors has the potential to yield extremely valuable information about not only the supernova process itself but also various aspects of fundamental physics of neutrinos themselves.

Neutrinos are detected through their weak charged current (CC) and neutral current (NC) interactions with

electrons and nuclei. There is a large body of literature on possible neutrino interaction channels that can be employed for detection of SN neutrinos; see, e.g. Refs. [7] (inverse beta decay), [8] (neutrino-electron scattering), [9, 10] (neutrino-nucleus scattering) and [11–14] (coherent elastic neutrino-nucleus scattering (CE ν NS)). Ref. [2] gives a comprehensive review and references on various neutrino processes and their cross sections in the context of supernova neutrino detection.

The NC process of CE ν NS has recently received much attention [15–19] in the context of large (multi-ton scale) detectors [20] searching for the weakly interacting massive particle (WIMP) candidates of dark matter (DM) [21] through WIMP-induced nuclear recoils (NR). In CE ν NS, neutrinos undergo coherent elastic scattering on the target nucleus with a cross section that is enhanced by the square of the number of neutrons in the target nucleus. The coherent enhancement of the cross section is of particular interest for SN neutrinos because of their relatively low energies (a few to a few tens of MeV) where the coherence effect is dominant. The recoiling target nucleus of mass M gets a maximum kinetic energy of $2E_\nu^2/M$, where E_ν is the neutrino energy. There is a trade-off between the cross section enhancement (requiring large mass nuclei) and the maximum recoil energy ($\propto 1/M$), with the latter typically in the region of a few keV for neutrino energy of ~ 10 MeV and target nuclei with mass number in the region

* pijush.bhattacharjee@saha.ac.in

† abhijit@rkmvu.ac.in

‡ sovan@iitg.ac.in

§ sayan.ghosh@saha.ac.in

¶ kamales.kar@gm.rkmvu.ac.in

** satyajit.saha@saha.ac.in

of ~ 100 desired for reasonably large cross section (typically, $O(10^{-39} \text{ cm}^2)$). Such low recoil energies, while very difficult to detect in conventional neutrino detectors, are, however, within reach of the large WIMP DM detectors. Thus, sufficiently large WIMP DM detectors with suitably chosen detector materials can also be sensitive to neutrinos from individual SN events. Importantly, the CE ν NS, it being a NC process, is equally sensitive to all flavors of neutrinos (and antineutrinos), which offers a probe for estimating the total explosion energy going into neutrinos [12, 15], and also possibly for demarcating the neutrinos originating in the different temporal phases of the neutrino emission during the SN event [18]. Because of these reasons, detailed calculations have been done studying the CE ν NS sensitivity of the next generation WIMP DM detectors, in particular, those using LXe as target detector material, to possible future nearby (Galactic) SN events; see, for example, Ref. [19].

In the present paper we show that, in addition to the NC process of CE ν NS, the future large LXe DM detectors would also be sensitive to inelastic CC interactions of the SN electron neutrinos (ν_e CC) with the xenon nuclei in the LXe detectors. Such interactions would produce a final state electron carrying a substantial fraction of the incident neutrino energy, and at the same time leave the post-interaction target nucleus in an excited state. Subsequent deexcitation of the latter would produce, among other particles, gamma rays and neutrons [22–26]. The electron and deexcitation gamma rays would give rise to signals similar to those seen for the “electron recoil” (ER) events [27] in DM detectors. These classes of signals will be designated as ν_e CC- e^- and ν_e CC- γ throughout this paper. At the same time, the “neutrino induced neutrons” (ν_e In) produced in the deexcitation of the post-interaction target nucleus would undergo elastic scattering on the target xenon nuclei and give rise to additional xenon nuclear recoils that, as we show below, may give significant contribution to observable NR signals at relatively large ($\gtrsim 30$ keV) recoil energies where the CE ν NS generated NR signal contribution is relatively small. In this paper we shall denote these ν_e In generated NR signals by ν_e CC- n .

Below we discuss the observable scintillation and ionization signals associated with the SN neutrino induced CE ν NS and ν_e CC events in a generic two-phase xenon detector using the GEANT4 [28] simulation toolkit, and study their detectability in future multi-ton scale LXe based DM detectors [20]. For simplicity, in this paper we consider only a single xenon isotope, namely, ^{132}Xe , for our calculations in order to illustrate the basic physical processes involved.

While both ν_e s and $\bar{\nu}_e$ s from the SN can undergo CC interactions with the xenon nuclei (the ν_μ s, $\bar{\nu}_\mu$ s, ν_τ s and $\bar{\nu}_\tau$ s can undergo only NC interaction because of insufficient incoming neutrino energies for production of the associated charged leptons), the contribution from $\bar{\nu}_e$ CC interaction with ^{132}Xe , which involves conversion of protons to neutrons inside the nucleus, is strongly suppressed

due to Pauli blocking of the neutron single particle states in the neutron rich final state nucleus [10]. Similarly, as seen in the case of ^{208}Pb [25], the contribution from the NC interaction of neutrinos and antineutrinos of all flavors with the target nuclei—in which the incoming neutrino or antineutrino only imparts energy to the neutrons and protons inside the nucleus without inducing interconversion between the nucleons—is also expected to be subdominant to the contribution from CC interactions of ν_e s for a target nucleus like ^{132}Xe with a moderately large neutron excess ($N - Z = 24$), again partly due to Pauli blocking effects. In the present paper, therefore, we only consider the ν_e CC interaction, i.e., the process $^{132}\text{Xe}(\nu_e, e^-)^{132}\text{Cs}^*$, for simplicity.

For the SN neutrino flux to be used for numerical calculations in this paper, we use the results of the Basel-Darmstadt (BD) simulations [29] of a $18M_\odot$ progenitor star placed at a distance of 1 kpc from earth for illustration of our results [30]. The instantaneous energy spectrum, SN neutrinos of type ν_i (with $\nu_i \equiv \nu_e, \bar{\nu}_e, \nu_\mu, \bar{\nu}_\mu, \nu_\tau, \bar{\nu}_\tau$) emitted (at the neutrinosphere) per unit time per unit energy is usually parametrized in terms of the time-dependent neutrino luminosities ($L_{\nu_i}(t)$), average energies ($\langle E_{\nu_i} \rangle(t)$), and the spectral shape parameter $\alpha_{\nu_i}(t)$ of the different neutrino flavors [31]. The temporal profiles of these parameters for different neutrino flavors extracted from the BD simulation results for the $18M_\odot$ progenitor SN used in this paper are given in graphical form in Refs. [18, 25, 32]. Note that the $\nu_\mu, \bar{\nu}_\mu, \nu_\tau, \bar{\nu}_\tau$ have essentially identical spectra and temporal profiles of their luminosities and average energies in the BD simulations.

For the CE ν NS process, since it is equally sensitive to all the neutrino species, the flavor oscillation effects are not relevant, and the time-integrated (over the duration of the SN burst event) sum of fluxes of all the neutrino species reaching the earth is same as the sum of the number of neutrinos of all species emitted (at the neutrinospheres) per unit time and energy, divided by $4\pi d^2$, d being the distance to the SN. On the other hand, the flux of ν_e s would in general depend on various flavor oscillation processes, including the standard Mikheyev-Smirnov-Wolfenstein (MSW) matter-enhanced neutrino flavor oscillation (see, e.g., [33]) as well as the phenomenon of collective neutrino flavor oscillations due to ν - ν interaction in the deep interior of the SN progenitor star; see, e.g., Refs. [3, 34–36]. However, as discussed in Refs. [32, 37], for the time-integrated fluxes of different neutrino species, the collective oscillation effects are small, and the fluxes of various neutrino species reaching the earth are given essentially by the MSW oscillations in the supernova matter. The resulting expressions for the ν_e and $\bar{\nu}_e$ fluxes at earth, for normal ordering (NO) and inverted ordering (IO) of the neutrino mass hierarchy are given in Refs. [25, 32], which we use in this paper. For simplicity, in this paper, we show all our numerical results for the NO case of neutrino mass hierarchy only; similar calculations can be done for the IO case.

The rest of the paper is arranged as follows: In Sec. II we set up the equations giving the differential recoil spectrum due to CE ν NS interaction of the SN neutrinos with the target nucleus. In Sec. III we discuss the inelastic CC interaction of ν_e s with ^{132}Xe nuclei, and calculate the energy spectrum of the electrons produced in the primary CC process $^{132}\text{Xe}(\nu_e, e^-)^{132}\text{Cs}^*$, as well as the energy spectra of the neutrons and γ -rays from deexcitation of the $^{132}\text{Cs}^*$ nuclei, for a $18M_\odot$ SN at a distance of 1 kpc from earth. The ^{132}Xe recoil spectrum due to multiple scattering of the neutrino-induced neutrons with the xenon nuclei is then calculated in Sec. IV using GEANT4 simulation. Sec. V discusses the observable scintillation and ionization signals due to (a) ^{132}Xe nuclear recoils originating from CE ν NS interactions and (b) ν_e CC origin electrons, γ -rays and neutrons (with the last one giving ^{132}Xe nuclear recoils) in a generic dual-phase LXe detector. The contributions of the different signal components associated with the CE ν NS and ν_e CC events are assessed and the possibility of distinguishing amongst them is discussed in Sec. VI. Finally, summary and conclusions are presented in Sec. VII.

II. SUPERNOVA NEUTRINO INDUCED XENON RECOIL SPECTRUM DUE TO CE ν NS

The differential cross section, $\frac{d\sigma}{dE_R}$, for the CE ν NS interaction of a neutrino of energy E_ν with a target nucleus of mass M which is left with a recoil (kinetic) energy E_R after the interaction is given by [11, 12, 17]

$$\frac{d\sigma}{dE_R} = \frac{G_F^2 M}{4\pi} Q_W^2 \left(1 - \frac{ME_R}{2E_\nu^2}\right) F^2(E_R), \quad (1)$$

where G_F is the Fermi constant, $Q_W = N - (1 - 4\sin^2\theta_W)Z$ is the weak nuclear hypercharge for the nucleus with N neutrons and Z protons, θ_W is the weak mixing angle (with $\sin^2\theta_W \simeq 0.2386$), and $F(E_R)$ is the nuclear form factor which we shall take to be of the Helm form [38],

$$F(E_R) = \frac{3j_1(qr_n)}{qr_n} e^{-q^2s^2/2}, \quad (2)$$

where j_1 is the spherical Bessel function, $q = (2ME_R)^{1/2}$ is the momentum transfer to the nucleus, $s \simeq 0.9$ fm is the nuclear skin thickness, $r_n^2 = c^2 + \frac{7}{3}\pi^2a^2 - 5s^2$ is the square of the effective nuclear radius with $c \simeq 1.23A^{1/3} - 0.60$ fm, $a \simeq 0.52$ fm, and $A = N + Z$.

The differential recoil spectrum, $\frac{dN_R}{dE_R}$, per ton (1000 kg) of target detector material (liquid ^{132}Xe , in our case) for the time-integrated (over the duration of the SN event) neutrino flux is then given by

$$\frac{dN_R}{dE_R} = N_{\text{Xe}} \sum_{\nu_i} \int_{E_\nu^{\min}} dE_\nu \frac{d\sigma}{dE_R} \Phi_{\nu_i}(E_\nu), \quad (3)$$

where the ν_i sum is over all six species of neutrinos, $E_\nu^{\min} = (ME_R/2)^{1/2}$ is the minimum energy of a neutrino that can produce a recoiling ^{132}Xe nucleus of recoil energy E_R , M being the mass of a ^{132}Xe nucleus, $N_{\text{Xe}} = 4.56 \times 10^{27}$ is the number of ^{132}Xe nuclei in one ton of liquid ^{132}Xe , and $\Phi_{\nu_i}(E_\nu)$ is the time-integrated flux of SN ν_i s per unit energy and per unit area at earth.

To facilitate easy comparison, the resulting ^{132}Xe recoil spectrum due to CE ν NS process for the BD $18M_\odot$ SN is displayed and discussed in section IV together with the recoil spectra due to the neutrons coming from the CC ν_e In process discussed in the next section.

III. INELASTIC CHARGED CURRENT INTERACTION OF SUPERNOVA NEUTRINOS WITH ^{132}Xe NUCLEI

The inelastic CC interaction of a supernova ν_e with a ^{132}Xe nucleus produces an electron and a ^{132}Cs nucleus in an excited state:

$$\nu_e + {}^{132}_{54}\text{Xe} \rightarrow e^- + {}^{132}_{55}\text{Cs}^*, \quad (4)$$

where the superscript $*$ stands for the excited state of the final state nucleus.

The differential cross section for this reaction in the $q \rightarrow 0$ limit (applicable for the energy range of SN neutrinos, q being the momentum transfer) can be written as [39–41]

$$\frac{d\sigma_{\nu_e}^{\text{CC}}}{dE_*} (E_\nu, E_*) = \frac{G_F^2 \cos^2\theta_c}{\pi} p_e E_e F(Z+1, E_e) \times [S_F(E_*) + (g_A^{\text{eff}})^2 S_{\text{GT}_-}(E_*)], \quad (5)$$

where G_F is the Fermi constant, θ_c is the Cabibbo angle, $E_* = E_\nu - E_e - Q$ is the excitation energy of the ^{132}Cs nucleus with $Q = M(^{132}_{55}\text{Cs}) - M(^{132}_{54}\text{Xe}) = 2.1263$ MeV [42], $M(^{132}_{55}\text{Cs})$ and $M(^{132}_{54}\text{Xe})$ being the masses of the two nuclei, E_ν is the incoming neutrino energy, and E_e and p_e are the energy and momentum of the emitted electron, respectively. The quantities $S_F(E_*)$ and $S_{\text{GT}_-}(E_*)$ are, respectively, the modulus squares of the averaged Fermi and Gamow-Teller (GT $_-$) transition matrix elements between the ground state of the initial nucleus $^{132}_{54}\text{Xe}$ and the excited state of the final nucleus $^{132}_{55}\text{Cs}^*$, and $g_A^{\text{eff}} \simeq 1.26$ is the ratio of the effective axial vector to vector coupling constants of the bare nucleon in the $q \rightarrow 0$ limit. The general expressions for $S_F(E_*)$ and $S_{\text{GT}_-}(E_*)$ are given in Refs. [39–41].

The factor $F(Z+1, E_e)$ in Eq. (5) is the correction factor which accounts for the distortion of the outgoing electron wave function due to Coulomb interaction with the final nucleus ($N-1, Z+1$) (with the initial nucleus represented as (N, Z)), and is given by [43]

$$F(Z, E_e) = 2(1+\gamma_0)(2p_e R)^{2(\gamma_0-1)} \times \frac{|\Gamma(\gamma_0 + iy)|^2}{|\Gamma(2\gamma_0 + 1)|^2} \exp(\pi y), \quad (6)$$

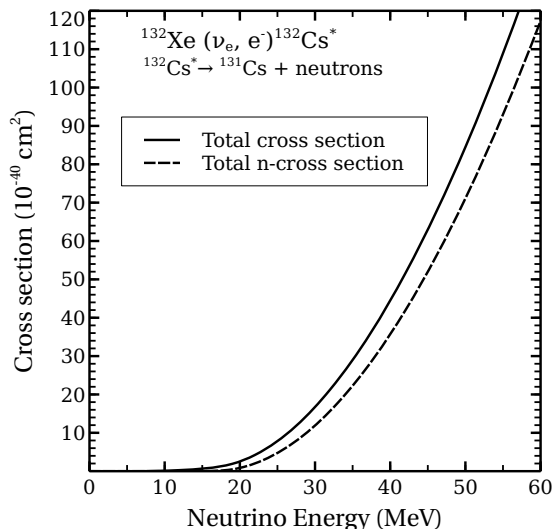


FIG. 1. Total cross section (solid curve) and neutron emission cross section (dashed curve) for the CC interaction of ν_e with ^{132}Xe as functions of the incoming neutrino energy.

where $\gamma_0 = (1 - Z^2\alpha^2)^{1/2}$, $y = \alpha ZE_e/p_e$, R is the radius of final nucleus and α the fine structure constant.

The Fermi transitions have the isospin selection rule $\Delta T = T' - T = 0$ where T' and T are, respectively, the isospins of the final and initial nucleus. Also, the Fermi strength sum over the final nucleus states is equal to $(N - Z)$, and it goes almost completely to the Isobaric Analog state (IAS) of the final nucleus with a very small spread in the neighboring states due to isospin breaking essentially by Coulomb interaction. The IAS in $^{132}\text{Cs}^*$ is at an excitation of 13.8 MeV [44]. On the other hand, the Gamow-Teller strength distribution is broad and its strength sum, which is slightly larger than $3(N - Z)$, is distributed over states with $T' = T - 1, T$ and $T + 1$, i.e., with $\Delta T = 1$. For the GT strength distribution S_{GT_-} for the final nucleus $^{132}\text{Cs}^*$ we use the results of a theoretical calculation [45] done within the deformed Hartree-Fock formalism using the density dependent Skyrme interaction Sk3 [46].

The reaction $^{132}\text{Xe}(\bar{\nu}_e, e^+)^{132}\text{I}^*$ initiated by the supernova $\bar{\nu}_e$ s also takes place, but the total GT strength, S_{GT_+} , for the reaction is $\simeq 0.51$ [45], which is only 0.7% of the total S_{GT_-} strength of $\simeq 72.12$ [45] for the reaction $^{132}\text{Xe}(\nu_e, e^-)^{132}\text{Cs}^*$ discussed above. Hence, in this paper we neglect the $\bar{\nu}_e$ CC contribution compared to the contribution from ν_e capture reaction.

The total cross section for ν_e CC interaction of a neutrino of energy E_ν with ^{132}Xe is obtained by integrating Eq. (5) over E_* , and is shown in Fig. 1 as a function of the incoming neutrino energy.

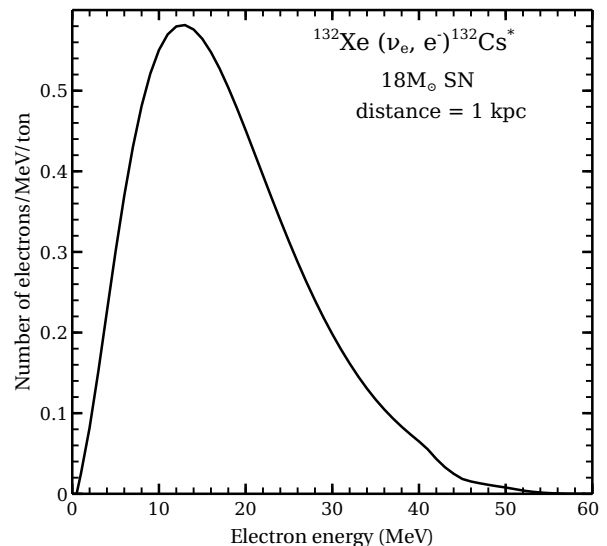


FIG. 2. Energy spectrum of electrons produced due to CC interaction of supernova ν_e s with ^{132}Xe nuclei, for the case of normal ordering (NO) of neutrino mass hierarchy, for SN neutrino flux given by the Basel-Darmstadt simulations [29] of a $18M_\odot$ progenitor supernova at a distance of 1 kpc.

A. Electron energy spectrum

The total energy spectrum of the electrons produced by the incident flux of SN ν_e s per ton of ^{132}Xe is given by

$$\frac{dN_{e,\text{total}}^{\text{CC}}}{dE_e} = N_{\text{Xe}} \int dE_\nu \Phi_{\nu_e}(E_\nu) \frac{d\sigma_{\nu_e}^{\text{CC}}(E_\nu, E_e)}{dE_e}, \quad (7)$$

where $\Phi_{\nu_e}(E_\nu)$ is the time-integrated flux (number per unit area per unit energy) of the SN ν_e s falling on the detector, $N_{\text{Xe}} = 4.56 \times 10^{27}$ is the number of ^{132}Xe nuclei in one ton of liquid ^{132}Xe , and $\frac{d\sigma_{\nu_e}^{\text{CC}}(E_\nu, E_e)}{dE_e}$ is given by Eq. (5) with $E_* = E_\nu - E_e - Q$. The resulting electron energy spectrum for the BD $18M_\odot$ SN ν_e flux is shown in Fig. 2. The total number of electrons produced is ~ 13.0 .

B. Energy spectrum of the neutrino induced neutrons ($\nu_e \text{In}$)

The final state excited nucleus $^{132}\text{Cs}^*$ can decay by emitting one or more neutrons:

$$^{132}\text{Cs}^* \rightarrow ^{131}\text{Cs} + n \quad \text{or} \quad ^{132}\text{Cs}^* \rightarrow ^{130}\text{Cs} + 2n, \quad (8)$$

and so on.

The emission of neutrons by the neutrino-induced excited nucleus can be considered as a two-step process involving two independent physical processes [23, 24]: the production of a final state excited nucleus due to absorption of the incoming neutrino by the target nucleus in the

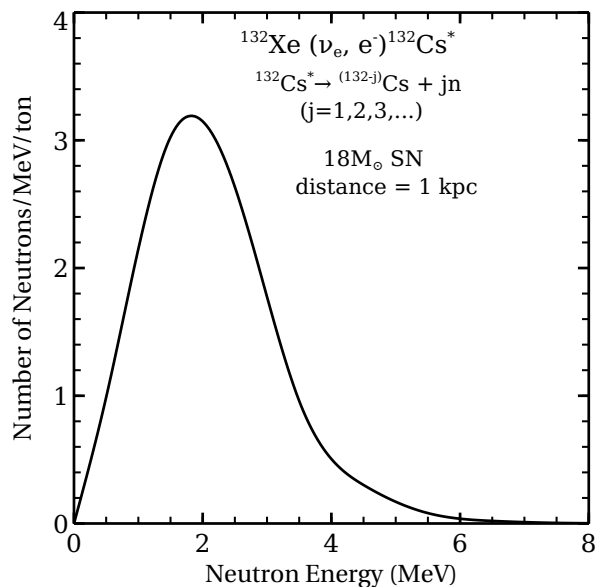


FIG. 3. Energy spectrum of neutrons emitted by excited ^{132}Cs nuclei produced due to inelastic CC interaction of supernova ν_e s with ^{132}Xe nuclei, for the case of normal ordering (NO) of neutrino mass hierarchy, for SN neutrino flux given by the Basel-Darmstadt simulations [29] of a $18M_{\odot}$ progenitor supernova at a distance of 1 kpc.

first step, and subsequent deexcitation of the final state nucleus through neutron emission in the second step.

The differential cross section for the first step, i.e., production of the excited ^{132}Cs nucleus due to ν_e capture on a target ^{132}Xe nucleus is given by Eq. (5). With this, the energy spectrum of the emitted neutrons is calculated in the following way: The differential cross section for emission of neutrons per unit neutron (kinetic) energy E_n by a single final state nucleus due to inelastic CC interaction of an incoming ν_e of energy E_{ν} with the target nucleus can be written as

$$\frac{d\sigma_{\nu_e}^{\text{CC},n}}{dE_n}(E_{\nu}, E_n) = \int \frac{d\sigma_{\nu_e}^{\text{CC}}}{dE_*}(E_{\nu}, E_*) \frac{dN_n}{dE_n}(E_*, E_n) dE_*, \quad (9)$$

where $\frac{dN_n}{dE_n}(E_*, E_n)$ is the energy spectrum of the neutrons produced by the excited nucleus of excitation energy E_* .

We calculate the neutron energy spectrum, $\frac{dN_n}{dE_n}(E_*, E_n)$, for $^{132}\text{Cs}^*$ using the fusion-evaporation Monte Carlo code PACE4 [47] originally developed by Gavron [48], including contributions from 1-, 2- and 3-neutron emissions. The total neutron emission cross section obtained by integrating Eq. (9) over E_n is shown in Fig. 1 as a function of the incoming neutrino energy, which can be compared with the total ν_e CC cross section shown in the same Figure.

The total energy spectrum of the neutrons produced

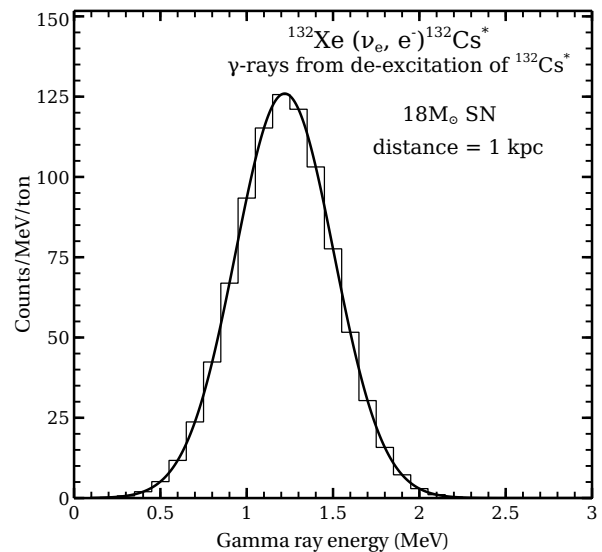


FIG. 4. Energy spectrum of deexcitation γ -rays emitted by excited ^{132}Cs nuclei produced due to inelastic CC interaction of supernova ν_e s with ^{132}Xe nuclei, for the case of normal ordering (NO) of neutrino mass hierarchy, for SN neutrino flux given by the Basel-Darmstadt simulations [29] of a $18M_{\odot}$ progenitor supernova at a distance of 1 kpc.

by the incident flux of SN neutrinos is then given by

$$\frac{dN_{n,\text{total}}^{\text{CC}}}{dE_n} = N_{\text{Xe}} \int dE_{\nu} \Phi_{\nu_e}(E_{\nu}) \frac{d\sigma_{\nu_e}^{\text{CC},n}}{dE_n}(E_{\nu}, E_n), \quad (10)$$

where $\Phi_{\nu_e}(E_{\nu})$ is the time-integrated flux spectrum (number per unit area per unit energy) of the SN ν_e s falling on the detector. The resulting neutron energy spectrum for the BD $18M_{\odot}$ SN ν_e flux for the NO case of neutrino mass hierarchy is shown in Fig. 3. The total number of neutrons produced is ~ 8.0 .

C. Energy spectrum of the neutrino induced γ -rays ($\nu_e \text{I}\gamma$)

The final state excited nucleus $^{132}\text{Cs}^*$ can also decay by emitting γ -rays. These gamma rays are of two types: discrete gamma rays arising from decays from higher energy bound states of the nucleus ($^{132}\text{Cs}^*$ in the present case) to lower energy ones, and statistical gamma rays having a continuous spectrum. The gamma rays of the latter type dominate and compete with the emission of neutrons and other light charged particles. While the discrete gamma rays predominantly have energy below 1 MeV, a calculation using the PACE code [47] gives a yield of continuum γ -rays that are concentrated in the energy range of ~ 1 – 2 MeV. Ignoring the discrete gamma rays, the average energy and average multiplicity of the deexcitation γ -rays from $^{132}\text{Cs}^*$ nuclei are found to be ~ 1.2 MeV and ~ 6 per ton of liquid ^{132}Xe , respectively, with a total number of γ -ray photons of ~ 90 , for the

same SN (mass $18M_{\odot}$) at a distance of 1 kpc as used in the calculation for neutron emission, for the case of normal ordering of neutrino mass hierarchy. The resulting spectrum of γ -rays is closely approximated by a gaussian with a mean at 1.22 MeV and FWHM of 0.67 MeV, and is shown in Fig. 4.

Inclusion of discrete gamma rays would slightly lower the mean energy, but this is effectively taken care of by increasing the width of the Gaussian distribution. On the other hand, the higher energy (> 2 MeV) part of the spectrum, which sums up to only $\lesssim 0.1\%$ of the contribution included in the spectrum, rapidly falls off with energy.

IV. XENON RECOIL SPECTRUM DUE TO SUPERNOVA NEUTRINO INDUCED NEUTRONS

The neutrons produced by inelastic CC interaction of the supernova ν_e s with target ^{132}Xe nuclei will scatter off the xenon nuclei themselves giving rise to recoiling ^{132}Xe nuclei. From Fig. 3 we see that the neutrons produced by the supernova neutrinos typically have energies of a few MeV with a spectrum peaking at ~ 2 MeV. At these neutron energies, elastic scattering dominates [49]. The mean-free-path (m.f.p) of neutrons of energies in the range of a few 100 keV to a few MeV in LXe is $O(10)$ cm. So, depending on the dimensions of the active volume of LXe and the point of production of the neutron within the detector, a neutron of a given initial energy may undergo multiple scattering within the detector giving rise to multiple xenon recoils with different recoil energies. To take this into account we perform a simulation of neutron scattering on xenon nuclei [50] using the GEANT4 simulation toolkit [28]. We use the GEANT4 Physics List *QGSP_BERT_HP* which, in addition to including all the standard electromagnetic processes, employs the high precision neutron package (*NeutronHP*) to transport neutrons below 20 MeV down to thermal energies [51].

A. GEANT4 simulation of neutron scattering on xenon nuclei

Guided by the typical designs of the LXe detectors being used in dark matter search experiments [20], we consider 1 ton of liquid ^{132}Xe contained in a cylindrical volume of aspect ratio (diameter-to-height) of 1:1. With a density of $\sim 2.953\text{ g/cm}^3$ of liquid xenon, both the diameter and height of the cylinder are taken to be ~ 75.4 cm. As far as the neutron induced xenon recoils are concerned, we find no significant differences in the results for the recoil spectra whether we consider natural xenon or one of its isotope (here ^{132}Xe). Neutrons of a given initial energy are generated homogeneously within the LXe volume with randomly chosen initial positions and with isotropic initial velocity directions.

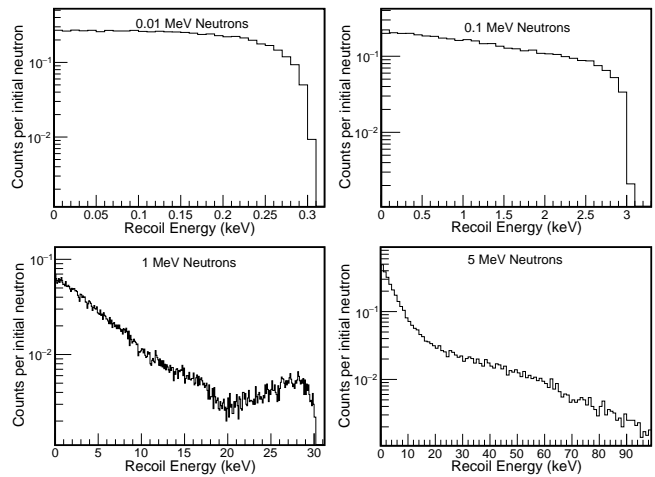


FIG. 5. ^{132}Xe recoil spectra generated by monoenergetic neutrons of different energies.

Although at the neutron energies of our interest the elastic scattering dominates [49], inelastic processes can also occur whereby, for example, the incident neutron is absorbed by a ^{132}Xe nucleus and re-emitted together with a gamma ray, resulting in a small recoil of the nucleus. The emitted neutron can then again scatter elastically or inelastically on another xenon nucleus depending on its energy, and so on. Each neutron is tracked until it hits and exits the outer boundary of the simulation volume or stops within the medium. Actually, given their large mean free paths, most neutrons in the energy range of the ν_e In spectrum shown in Fig. 3 would be scattered out of the detector volume after undergoing single or multiple scattering.

To understand the nature of the final recoil spectrum, we first study the recoil spectra generated by initially monoenergetic neutrons. Fig. 5 shows the xenon recoil spectra for four different initial energies of neutrons, namely, 0.01, 0.1, 1 and 5 MeV. It is seen that while at very low energies the recoil spectrum is almost flat, the spectrum becomes increasingly skewed towards low recoil energies as the initial neutron energy increases. This directly reflects the behavior of the angular distribution of the recoiling nucleus in the elastic scattering of neutrons on ^{132}Xe nuclei, with relatively more number of forward (small angle) scattering taking place than backward scattering as the neutron energy increases [49].

Next, we show in Fig. 6 the probability distribution of the number of ^{132}Xe recoils produced by neutrons of different initial energies. It can be seen that for all initial neutron energies, 1–2 scattering events dominate, with the probability of larger number of scattering falling off faster with number of scatterings for increasing initial energy of the neutron. Note, however, that the multiple scattering events (greater than 1–2 scatterings), although less probable than 1–2 scattering events, can still contribute significantly to the total recoil spectrum because each such scattering produces a larger number of recoils

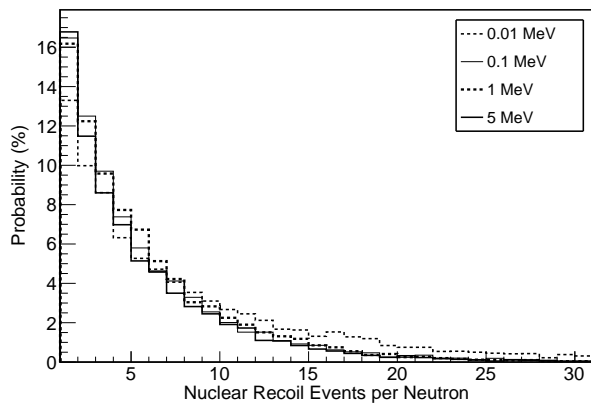


FIG. 6. Distribution of the number of ^{132}Xe recoils produced (i.e., the number of scatterings suffered) by monoenergetic neutrons of various energies.

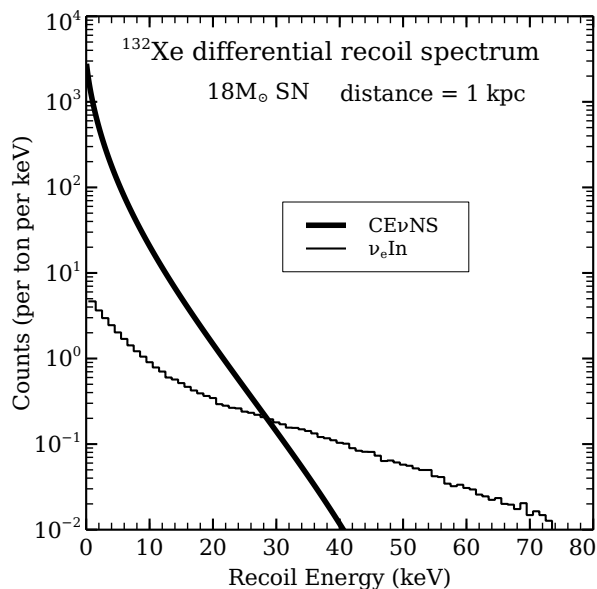


FIG. 7. ^{132}Xe differential recoil spectrum due to supernova neutrino induced $\text{CE}\nu\text{NS}$ (curve marked “ $\text{CE}\nu\text{NS}$ ”) and the spectrum due to neutrons produced by inelastic CC interaction of supernova ν_e s with ^{132}Xe nuclei (curve marked “ $\nu_e\text{In}$ ”) for the case of normal ordering of neutrino mass hierarchy shown in Fig. 3. Both the curves correspond to SN neutrino flux given by the Basel-Darmstadt simulations [29] of a $18M_\odot$ supernova progenitor at a distance of 1 kpc.

per initial neutron than the 1–2 scattering events.

The final differential recoil spectrum generated by the SN ν_e induced neutrons whose initial energies are randomly sampled from the spectrum shown in Fig. 3 is shown in Fig. 7 together with the direct recoil spectrum of ^{132}Xe due to the $\text{CE}\nu\text{NS}$ process given by Eq. (3). From Fig. 7 we see that the $\nu_e\text{In}$ generated xenon recoils associated with the $\nu_e\text{CC}$ events can in principle give a significant contribution to the total observable NR signal at relatively large ($\gtrsim 30$ keV) recoil energies where

the $\text{CE}\nu\text{NS}$ generated NR signal contribution is relatively small.

V. OBSERVABLE SIGNALS IN DUAL-PHASE XENON DETECTORS

A typical dual-phase (liquid-gas) xenon detector consists of a cylindrical time projection chamber (TPC) containing liquid xenon, with a layer of gaseous xenon at the top. The energy deposited due to a particle interaction within the TPC is dissipated in the liquid xenon medium through various modes including excitation and ionization of the xenon atoms, and heat dissipation. This gives rise to two observable signals: (a) a prompt scintillation light signal (S1) associated with deexcitation of the excited xenon molecular states and (b) a delayed light signal associated with the ionization electrons which are drifted through the liquid xenon by an applied vertical electric field and extracted (by a second, relatively stronger electric field) into the xenon gas layer at the top where they give rise to a secondary, “proportional scintillation” signal (S2) (it being proportional to the number of extracted ionization electrons) by collision with xenon atoms. Both these light signals are detected with two arrays of photomultiplier tubes (PMTs), one placed at the top and the other at the bottom of the TPC. In terms of the number of photoelectrons (PEs) produced in the PMTs, the S2 signal is generally significantly larger than S1 (by factors ranging from a few tens to a few hundreds depending on the energy deposition) due to amplification characteristic of the proportional scintillation process. Detection of both S1 and S2 signals from the same energy deposition event gives a dual-phase TPC the ability to reconstruct the 3D location of the energy deposition event within the TPC, while the measured S1-to-S2 ratio allows effective discrimination between NR signals (due to dark matter, background neutrons, for example) and ER signals (due to background β and γ particles).

Below we discuss the observable S1 and S2 signals due to $\text{CE}\nu\text{NS}$ origin xenon nuclear recoils and $\nu_e\text{CC}$ origin neutrons (which generate xenon nuclear recoils), electrons and γ -rays, in a generic dual-phase LXe detector. The contributions of the different signal components associated with the $\text{CE}\nu\text{NS}$ and $\nu_e\text{CC}$ events are assessed and the possibility of distinguishing amongst them is discussed in Sec. VI below. The basic physics we follow for working out these signals is that described in the Noble Element Simulation Technique (NEST) model [52–54], which gives a semi-empirical method of estimating the yields of scintillation photons and ionization electrons produced by recoiling particles in LXe. Because of the basic difference in the nature of energy deposits by NRs and ERs, the scintillation and ionization yields differ in the two cases, and consequently, the S1 and S2 signal generation procedures are somewhat different in the two cases. In this paper we are interested in obtaining only the strengths of the signals in a generic detector and not

detailed detector specific simulations. As such we follow the simplified treatment described in Refs. [19, 27] together with GEANT4 simulation (for propagation and tracking of the relevant particles inside the detector) for obtaining the S1 and S2 signal strengths. For the NRs, we use the same light and ionization yields as those used in Ref. [55] and detector parameters (like those specifying S1 and S2 gains, drift time of the ionization electrons, and so on) as those used in Ref. [19]. For the ER case, we use the benchmark results for the light and ionization yields using the publicly available NEST code [56], while the detector parameters are taken to be the same as those used for the NR case. More details of our simulation procedure are given in Ref. [57].

A. S1 and S2 signals from $\text{CE}\nu\text{NS}$ and $\nu_e\text{CC}$ origin nuclear recoils

The S1 and S2 differential spectra due to $\text{CE}\nu\text{NS}$ and $\nu_e\text{CC}$ origin NRs are generated from the corresponding differential recoil energy spectrum shown in Fig. 7.

For the $\text{CE}\nu\text{NS}$ process, a given incoming neutrino may be expected to interact, if at all, only once within the detector volume and thus generate only one xenon nuclear recoil, which gives one S1 and one S2 signal for each $\text{CE}\nu\text{NS}$ interaction. On the other hand, a single neutron produced in the $\nu_e\text{CC}$ process may undergo multiple scattering giving rise to multiple xenon recoils along its track, which would in general give rise to multiple S1 and S2 signals associated with a single neutron. However, due to different nature of their origin, the construction of the final observable S1 spectrum must be treated differently from that of S2.

First, we note that the typical signal sampling rate in currently operating large LXe detectors is about 1 sample per 10 ns, a time scale that is much larger than the light travel time scale across the detector volume. So, in the case of S1, it being a prompt signal, the arrival time difference (at the PMT arrays) between S1 photons originating from two successive interaction vertices of a neutron is essentially the same as the time interval between the two successive interactions. The typical width of an individual S1 pulse is about 27 ns [58] (fixed by the mean deexcitation lifetime of the excited xenon atoms). So any two S1 signals associated with two neutron scattering events originating within say 50 ns of each other will overlap and cannot be distinguished. A neutron of initial energy of ~ 2 MeV (corresponding to the peak of the neutron spectrum shown in Fig. 3) has a speed of ~ 2 cm/ns. With a mean free path of ~ 13 cm in liquid xenon, the mean time between two successive scatterings of such a neutron is ~ 6.5 ns. This implies that multiple S1 signals from neutron scattering events separated by less than 7–8 mean free paths would be unresolvable and will be merged. At the same time, as seen from Fig. 6, the probability for a neutron undergoing more than 7–8 scatterings is relatively small unless the initial neutron

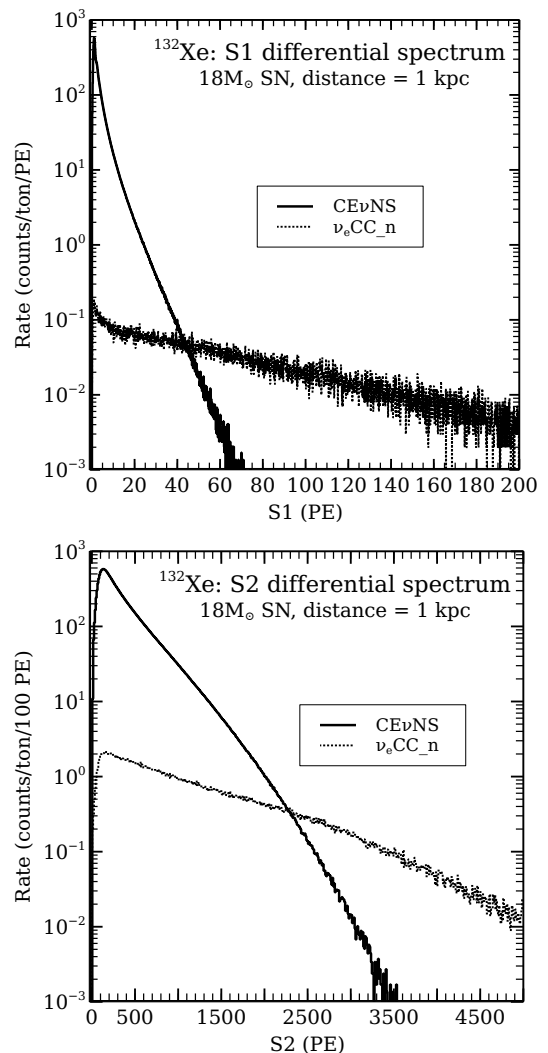


FIG. 8. The observable S1 (upper panel) and S2 (lower panel) differential spectra corresponding to the ^{132}Xe recoil spectra shown in Fig. 7.

energy is significantly smaller than 2 MeV and the detector scale size is significantly larger (> 1 m). Based on these considerations, in our simulation program the S1 signals (PEs) due to multiple scattering of each neutron (sampled from the spectrum shown in Fig. 3) are merged into one S1 signal.

On the other hand, the S2 signals are produced by the ionization electrons colliding with the xenon atoms in the gas phase, the electrons being originally produced in the liquid xenon bulk of the TPC and then drifted in the vertical (z) direction through the liquid xenon and finally extracted into the gas phase by another external electric field. With a typical drift speed of the electrons of ~ 2 mm/ μs through liquid xenon, the arrival time difference at the gas phase between two sets of ionization electrons originating from two successive neutron scattering events (occurring in the liquid xenon) can be \sim a fraction of a μs to a few hundreds of μs (depending on the

difference in the z positions of the two neutron scattering vertices in the liquid and the dimensions of the detector), compared to a few ns time scale between two successive scattering of a neutron in the liquid xenon. Given that observed S2 signal pulses have typical widths of $\sim 1\text{--}2\ \mu\text{s}$ [59], in our simulation, therefore, the S2 signals (PEs) due to electrons arriving in the gas phase within a $2\ \mu\text{s}$ window were combined into a single S2 signal, while those due to the electrons reaching the gas phase beyond this window were treated as separate ones. The resulting S1 and S2 differential spectra due to ^{132}Xe recoils originating from $\text{CE}\nu\text{NS}$ and $\nu_e\text{In}$ processes (Fig. 7) are shown in Fig. 8.

B. S1 and S2 signals from electrons and deexcitation gamma rays

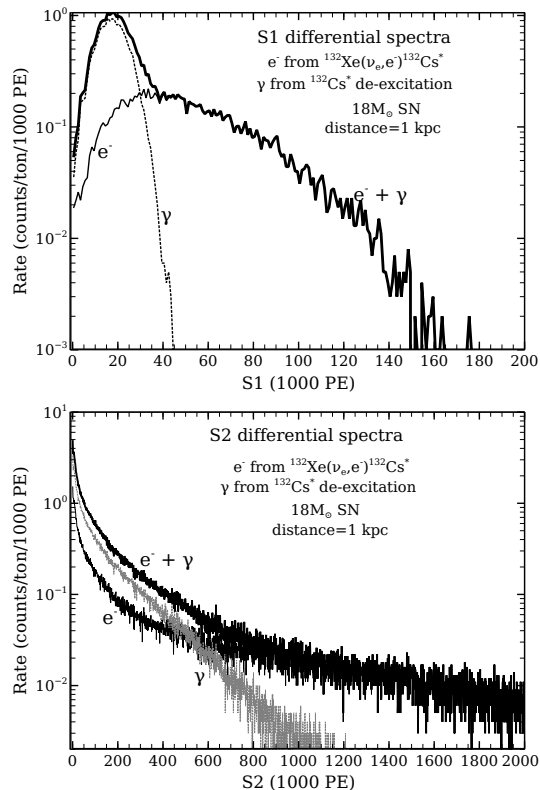


FIG. 9. The observable S1 (upper panel) and S2 (lower panel) differential spectra due to electrons generated in the CC process $^{132}\text{Xe}(\nu_e, e^-)^{132}\text{Cs}^*$ and γ -rays from deexcitation of the $^{132}\text{Cs}^*$ nuclei, corresponding to their energy spectra shown in Figs. 2 and 4, respectively.

The energy spectra of the electrons produced in the primary CC process $^{132}\text{Xe}(\nu_e, e^-)^{132}\text{Cs}^*$ and the γ -rays from deexcitation of the $^{132}\text{Cs}^*$ nuclei are shown in Figs. 2 and 4, respectively. While the low energy electrons create further ionization electrons, the high energy ones create Bremsstrahlung γ -rays, which together with the original

γ -rays undergo Compton and photoelectric interactions with electrons in the xenon atoms and produce further energetic electrons. We perform GEANT4 simulations to propagate and track all the electrons and gamma rays whose initial energies are randomly sampled from their energy spectra shown in Figs. 2 and 4, respectively, and then generate their S1 and S2 signals by the procedure outlined above. It is observed that although each electron or γ -ray undergoes many interactions, all these interactions occur within a small region (within a few mm to few cm depending on the energy of the particle) around their production points. For reasons explained in Sec. V A, this effectively gives rise to one S1 signal and about 1–3 S2 signals (after taking into account the effect of merging of S2 signals) for every electron or γ -ray.

The resulting S1 and S2 differential spectra generated by the electrons and γ -rays are shown in Fig. 9

VI. CONTRIBUTIONS OF DIFFERENT EVENT TYPES AND THEIR DISTINGUISHABILITY IN THE OBSERVED SIGNALS

In a SN burst event, a LXe detector would in general record both the $\text{CE}\nu\text{NS}$ events due to NC interaction of all species of SN neutrinos with the xenon nuclei and the $\nu_e\text{CC}$ events due to CC interaction of the ν_e s with the xenon nuclei. The $\text{CE}\nu\text{NS}$ events generate signals characteristic of nuclear recoils whereas the $\nu_e\text{CC}$ events in general have two signal components: (a) the “ $\nu_e\text{CC}_-(e^- + \gamma)$ ” component due to electrons generated in the CC process $^{132}\text{Xe}(\nu_e, e^-)^{132}\text{Cs}^*$ and additionally due to γ -rays from deexcitation of the final state $^{132}\text{Cs}^*$ nuclei, and (b) the “ $\nu_e\text{CC}_n$ ” component due to xenon nuclear recoils caused by the scattering of neutrons off the xenon nuclei, the neutrons being from deexcitation of the final state $^{132}\text{Cs}^*$ nuclei.

In order to see the contribution of different event types in the final observed number of events, we show in Fig. 10 the number of events as functions of S1 and S2 PE thresholds obtained by respectively integrating the differential S1 and S2 spectra shown in Figs. 8 and 9 for different values of S1 and S2 thresholds, respectively.

Note that S2 signals are in general significantly larger than S1 signals by at least an order of magnitude both in terms of number of photoelectrons in individual signal events as well as in terms of integral number of events (counts/ton) as function of the relevant PE threshold.

It is clear that $\nu_e\text{CC}_-(e^- + \gamma)$ signals largely dominate the overall observed signals in both S1 and S2 except for relatively low detector thresholds with S1 threshold, $S1_{\text{th}} \lesssim 15$, and S2 threshold $S2_{\text{th}} \lesssim 700$ PEs, for which $\text{CE}\nu\text{NS}$ origin NR signals dominate. This indicates that upcoming large, multi-ton class LXe based DM detectors will be strongly sensitive to the $e^- + \gamma$ signal arising from $\nu_e\text{CC}$ events caused by SN ν_e s in addition to the nuclear recoil signal due to the $\text{CE}\nu\text{NS}$ events arising from NC interactions of all the six neutrino species. The

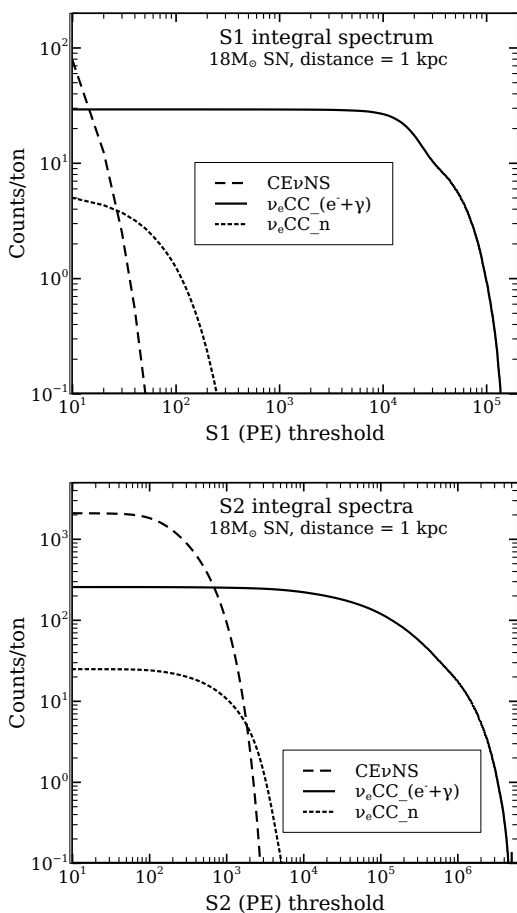


FIG. 10. Contributions of different signal components to the observable S1 (upper panel) and S2 (lower panel) signals as functions of the S1 (PE) and S2 (PE) threshold, respectively, per ton of liquid ^{132}Xe . These are obtained by respectively integrating the differential S1 and S2 spectra shown in Figs. 8 and 9 for different values of S1 and S2 thresholds.

usual problem of ER and NR backgrounds encountered in DM search may be largely mitigated in the case of SN neutrinos due to relatively short duration ($\sim O(10)\text{s}$) of the SN burst event. Note that the ν_e In-induced NR signal ($\nu_e\text{CC}_n$) is subdominant to both $\text{CE}\nu\text{NS}$ -induced NR and $\nu_e\text{CC}_-(e^- + \gamma)$ signals.

From the estimated numbers of various types of signals shown in Fig. 10, and nominally scaling these numbers with active detector mass (M_{Det}) and distance (d) to the SN as M_{Det}/d^2 , we see that with a future large LXe detector of the class of the proposed DARWIN [20] detector, for example, with an active target mass of ~ 40 ton, we may expect $\sim [839, 103, 10]$ S2 signals due to $[\text{CE}\nu\text{NS}, \nu_e\text{CC}_-(e^- + \gamma), \nu_e\text{CC}_n]$ above S2 thresholds of 10 PEs, for the $18M_{\odot}$ SN at a distance of 10 kpc. For a S2 threshold of $S2_{\text{th}} = 100$ and 1000 PEs, these numbers are $\sim [730, 103, 9]$ and $\sim [37, 101, 4]$, respectively. Similar scaling of expected number of signals with detector mass and SN distance can be obtained for S2 as well as

S1 for various S2 and S1 PE thresholds.

An important question to consider is whether it would be possible to distinguish the individual signal components ($\text{CE}\nu\text{NS}$, $\nu_e\text{CC}_-(e^- + \gamma)$, $\nu_e\text{CC}_n$) within a given total number of observed events. This is important because, while the number of $\text{CE}\nu\text{NS}$ events is sensitive to all six neutrino species, those of the two signal components of $\nu_e\text{CC}$ events ($\nu_e\text{CC}_-(e^- + \gamma)$ and $\nu_e\text{CC}_n$) are both sensitive only to ν_e s. Identification of each signal component in the total number of observed events would therefore provide a good handle on the flavor composition of the total SN neutrino flux.

In this context, note first that, since the $\nu_e\text{CC}$ and the $\text{CE}\nu\text{NS}$ events result from different underlying fundamental interaction processes, the occurrence of these two types of events would in general be separated in time. On the other hand, for a given $\nu_e\text{CC}$ interaction event, the prompt S1 signals due to $\nu_e\text{CC}_-(e^- + \gamma)$ and $\nu_e\text{CC}_n$ will be temporally superimposed on each other, and will be registered as a single combined S1 response, thus rendering them indistinguishable. However, the following considerations with regard to the S2 signals may still offer a possible way to separate the $\nu_e\text{CC}_-(e^- + \gamma)$ and $\nu_e\text{CC}_n$ signals, at least on a statistical basis, though perhaps not on event-by-event basis:

In general, a particle (electron, gamma ray or neutron) produced in a $\nu_e\text{CC}$ interaction event will undergo multiple scattering whereby the particle would deposit a part of its energy (through production of a bunch of ionization electrons which eventually produce the S2 signals) at each “hit-point”, i.e., a point of interaction with a scatterer (e.g., a xenon nucleus or an electron) along its track. Since the ranges of the electrons and γ -rays of the relevant energies are of the order of a few mm to a few cm in LXe [60], the majority of these “hit-points” would be located very close (within a few cm) to their corresponding $\nu_e\text{CC}$ interaction points where the electrons and gamma rays are originally generated. In contrast, the neutrons mainly lose energy through multiple scatterings on the xenon nuclei, thereby producing recoiling xenon nuclei which, in turn, produce the ionization electrons. Since the mean free path lengths of the neutrons in LXe is relatively large ($O(10)$ cm), it is expected that the hit-points for neutrons would in general be located further away (compared to those for electrons and gamma rays) from the corresponding $\nu_e\text{CC}$ interaction points where the neutrons are generated. This can be seen from Fig. 11 which shows the distribution of all the hit points (marked by their distances from the corresponding $\nu_e\text{CC}$ interaction vertices) for neutrons, electrons and gamma rays, obtained from our GEANT4 simulation. Clearly, the hit-point distribution of the neutrons is broader, and the neutrons’ energy deposition points are spatially more widely spread out, than those for electrons and gamma rays. Since the LXe TPCs generally have the capability of hit-point position reconstruction using the S2 signals from the arrays of PMTs above the gas phase of the TPC, a suitable algorithm similar to the one used for (x,y)

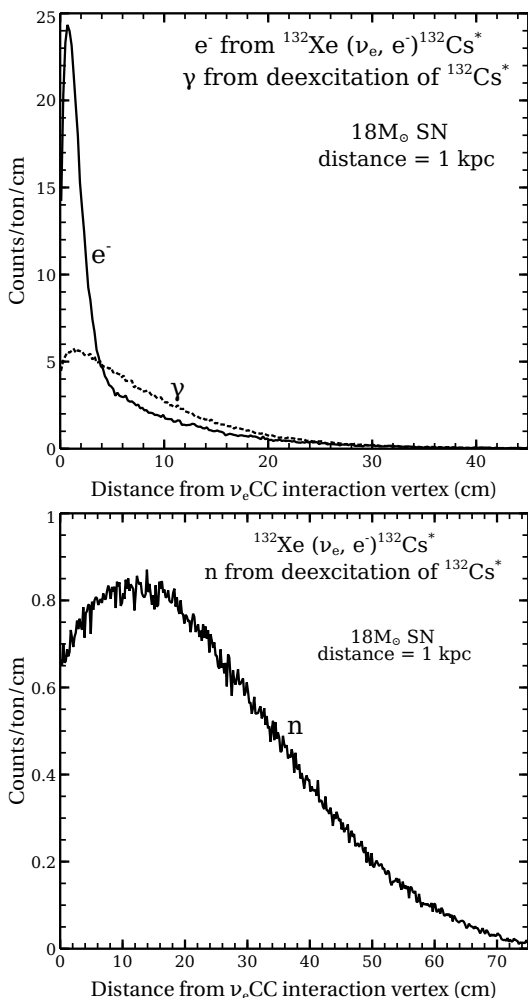


FIG. 11. Hit-point distribution for electrons and gamma rays (upper panel) and neutrino-induced neutrons (lower panel) from ν_e CC interactions.

position reconstruction of the hit-points (as discussed, for example, in Sec. II.B of Ref. [61]) could in principle be used to distinguish between the ν_e CC $_{-}(e^- + \gamma)$ and ν_e CC $_{-}n$ signals, at least on a statistical basis, provided that corresponding S2 signals of the two event subclasses are temporally separable, i.e., the corresponding track projections are well separated along the TPC drift (z) axis. Indeed, from a simple integration of the distance distributions shown in Fig. 11 for various threshold distances, one finds, for example, that more than 75% of the neutron hit-points lie beyond a distance of 10 cm from the corresponding ν_e CC interaction vertices, whereas the fractions of gamma ray and electron hit points that lie beyond 10 cm from the corresponding ν_e CC interaction vertices are only $\sim 17\%$ and 32% , respectively, with the rest (83% and 68%, respectively) of the hit points lying inside 10 cm. Of course, to see how exactly these different hit-point distributions at the energy deposition level in the bulk of the TPC translate to different spatial distributions of the PMT hit patterns at the PMT array

plane at the top of the gas phase, will require detailed detector specific simulations, which is beyond the scope of the present paper.

At this point it is worth mentioning that there is also an additional channel for possible identification of the neutrons generated in the ν_e CC interactions. This comes from the consideration that a large fraction of the neutrons associated with the ν_e CC events may not be stopped within the LXe tank, and may escape the detector volume with residual energies. Indeed, our neutron tracking simulation described in Sec. IV A shows this escaping neutron fraction to be more than 90%. An array of suitable neutron detectors placed around the detector volume (see.e.g., Ref. [62]) may, therefore, be utilized to detect the escaping neutrons in coincidence, thereby identifying the ν_e CC origin neutrons. Again, the relevant neutron background is expected to be small over the duration of the SN burst event.

Both the possibilities mentioned above are, however, challenging propositions that can be fully addressed and established only by means of detailed simulations using, for example, an “event generator” similar to those used in neutrino physics (see, e.g., Ref. [63]), together with detailed detector simulations, which can be the subject of a future work.

VII. SUMMARY AND CONCLUSIONS

Several previous studies have shown that future large, multi-10 tonne class, LXe detectors for dark matter search will also be sensitive to supernova neutrino induced xenon nuclear recoils due to the $\text{CE}\nu\text{NS}$ process, which involves NC interactions of all six species of neutrinos including their antineutrinos. In this paper we have pointed out that the same LXe based detectors will also be sensitive to inelastic charged current (CC) interactions of the SN electron neutrinos with the xenon nuclei. In such interactions, an electron is produced in the final state and the post-interaction target nucleus is left in an excited state, the subsequent deexcitation of which produces, among other particles, gamma rays and neutrons. The electron and deexcitation gamma rays would give rise to electron recoil type signals (ν_e CC $_{-}(e^- + \gamma)$) while neutrons from the deexcitation of the post-interaction nuclei—the so called neutrino induced neutrons—would produce additional xenon nuclear recoils (i.e., in addition to $\text{CE}\nu\text{NS}$ generated NRs) through (multiple) scattering of the neutrons with the xenon nuclei and produce NR type signals (ν_e CC $_{-}n$).

We have estimated the relative contributions of the three different signal components ($\text{CE}\nu\text{NS}$, ν_e CC $_{-}(e^- + \gamma)$, ν_e CC $_{-}n$) to the total observable scintillation and ionization signals in a generic two-phase LXe detector. We have also discussed possible ways to identify the individual event types in the total number of observed events.

It is found that in terms of the number of PEs produced in individual PMTs, the largest signals—both scin-

tillation (S1) and ionization (S2) signals—come from the combined contribution due to the electrons generated in the $\nu_e\text{CC}$ process $^{132}\text{Xe}(\nu_e, e^-)^{132}\text{Cs}^*$ and the γ -rays from deexcitation of the $^{132}\text{Cs}^*$ nuclei. In terms of event counts (number of events per tonne of active detector mass), the $\text{CE}\nu\text{NS}$ events dominate the total event counts for relatively low detector thresholds of $S1_{\text{th}} \lesssim 15$ and $S2_{\text{th}} \lesssim 700$ PEs, whereas the $\nu_e\text{CC}-(e^- + \gamma)$ component of the $\nu_e\text{CC}$ events dominate for larger thresholds. The $\nu_e\text{CC}_n$ component of the $\nu_e\text{CC}$ event signals remains subdominant to both the $\nu_e\text{CC}-(e^- + \gamma)$ and $\text{CE}\nu\text{NS}$ signals throughout the S1 and S2 PE ranges under consideration. Moreover, in general, the prompt S1 signals corresponding to the $\nu_e\text{CC}-(e^- + \gamma)$ and $\nu_e\text{CC}_n$ signal components of any given $\nu_e\text{CC}$ event will temporally be superimposed on each other, rendering them indistinguishable if only S1 signal is considered. However, it may still be possible to separate these two signal components, at least on a statistical basis, based on the expected different spatial distributions of the PMT hit patterns for

the S2 signals from $\nu_e\text{CC}-(e^- + \gamma)$ and $\nu_e\text{CC}_n$. In addition, since a large fraction of the neutrons generated in the $\nu_e\text{CC}$ events are likely to escape the detector volume with significant amount of residual energies, coincidence detection of these escaping neutrons by means of a suitable arrangement of neutron veto detectors may provide an additional channel for identifying the $\nu_e\text{CC}$ origin neutrons. Detection and identification of the $\nu_e\text{CC}$ events due to SN ν_e CC interactions together with the $\text{CE}\nu\text{NS}$ events generated through NC interaction of all neutrino species in future multi-10 tonne class LXe detectors may provide a good probe for extracting useful information about the distribution of the total SN explosion energy going into different neutrino flavors.

Acknowledgment: We thank the three anonymous referees for useful comments and constructive suggestions for improvement of the manuscript. We thank Rafael Lang for useful suggestions. One of us (SG) thanks Will Taylor for useful correspondence. Two of us (PB and SS) acknowledge support for this work under the Raja Ramanna Fellowship program of the Department of Atomic Energy (DAE), Government of India.

-
- [1] H.A. Bethe, *Rev. Mod. Phys.* **62**, 801 (1990); H.-T. Janka, *Annu. Rev. Nucl. Part. Sci.* **62**, 407 (2012); A. Burrows, *Rev. Mod. Phys.* **85**, 245 (2013); S. Smartt, *Publ. Astron. Soc. Aust.* **32**, e016 (2015); B. Müller, *Publ. Astron. Soc. Aust.* **33**, e048 (2016); H.-T. Janka, T. Melson, and A. Summa, *Annu. Rev. Nucl. Part. Sci.* **66**, 341 (2016); A. Mirizzi, I. Tamborra, H.-T. Janka, N. Saviano, K. Scholberg, R. Bollig, L. Hüdepohl, and S. Chakraborty, *Riv. Nuovo Cimento* **39**, 1 (2016) [arXiv:1508.00785].
- [2] K. Scholberg, *Annu. Rev. Nucl. Part. Sci.* **62**, 81 (2012).
- [3] A. Mirizzi *et al.* in Ref. [1].
- [4] S.W. Li, L.F. Roberts, and J.F. Beacom, *Phys. Rev. D* **103**, 023016 (2021).
- [5] K. Abe *et al.* (Super-Kamiokande Collaboration), *Phys. Rev. D* **94**, 052010 (2016); B. Abi *et al.* (DUNE Collaboration), arXiv:2008.06647; F. An *et al.* (JUNO Collaboration), *J. Phys. G* **43**, 030401 (2016); K. Abe *et al.* (Hyper-Kamiokande Collaboration), arXiv:1805.04163; C.A. Duba *et al.* (HALO Collaboration), *J. Phys. Conf. Ser.* **136**, 042077 (2008); D. Väänänen and C. Volpe, *J. Cosmol. Astropart. Phys.* **10(2011)** 019.
- [6] K. Hirata *et al.* (KAMIOKANDE-II Collaboration), *Phys. Rev. Lett.* **58**, 1490 (1987); *Phys. Rev. D* **38**, 448 (1988); R.M. Bionta *et al.*, *Phys. Rev. Lett.* **58**, 1494 (1987); C.B. Bratton *et al.*, *Phys. Rev. D* **37**, 3361 (1988); E.N. Alekseev, L.N. Alekseeva, I.V. Krivosheina, and V.I. Volchenko, *Phys. Lett. B* **205**, 209 (1988); V.L. Dadykin *et al.*, *JETP Lett.* **45**, 593 (1987); M. Aglietta *et al.*, *Europhys. Lett.* **3**, 1315 (1987).
- [7] P. Vogel and J.F. Beacom, *Phys. Rev. D* **60**, 053003 (1999); A. Strumia and F. Vissani, *Phys. Lett. B* **564**, 42 (2003); J.F. Beacom and M.R. Vagins, *Phys. Rev. Lett.* **93**, 171101 (2004).
- [8] W.J. Marciano and Z. Parsa, *J. Phys. G* **29**, 2629 (2003).
- [9] R.S. Raghavan, *Phys. Rev. D* **34**, 2088 (1986); W.C. Haxton, *Phys. Rev. D* **36**, 2283 (1987); K. Langanke, P. Vogel, and E. Kolbe, *Phys. Rev. Lett.* **76**, 2629 (1996); J. Toivanen, E. Kolbe, K. Langanke, G. Martínez-Pinedo, and P. Vogel, *Nucl. Phys. A* **694**, 395 (2001).
- [10] E. Kolbe, K. Langanke, G. Martínez-Pinedo, and P. Vogel, *J. Phys. G: Nucl. Part. Phys.* **29**, 2569 (2003); N. Jachowicz, N. Van Dessel, and A. Nikolakopoulos, *J. Phys. G: Nucl. Part. Phys.* **46**, 084003 (2019).
- [11] D.Z. Freedman, *Phys. Rev. D* **9**, 1389 (1974); D.Z. Freedman, D.N. Schramm, and D.L. Tubbs, *Annu. Rev. Nucl. Sci.* **27**, 167 (1977).
- [12] A. Drukier and L. Stodolsky, *Phys. Rev. D* **30**, 2295 (1984).
- [13] B. Cabrera, L.M. Krauss, and F. Wilczek, *Phys. Rev. Lett.* **55**, 25 (1985).
- [14] COHERENT Collaboration: D. Akimov *et al.*, *Science* **357**, 1123–1126 (2017).
- [15] C.J. Horowitz, K.J. Coakley, and D.N. McKinsey, *Phys. Rev. D* **68**, 023005 (2003).
- [16] J. Monroe and P. Fisher, *Phys. Rev. D* **76**, 033007 (2007); L.E. Strigari, *New J. Phys.* **11**, 105011 (2009).
- [17] A.J. Anderson, J.M. Conrad, E. Figueroa-Feliciano, K. Scholberg, and J. Spitz, *Phys. Rev. D* **84**, 013008 (2011).
- [18] S. Chakraborty, P. Bhattacharjee, and K. Kar, *Phys. Rev. D* **89**, 013011 (2014).
- [19] R.F. Lang, C. McCabe, S. Reichard, M. Selvi and I. Tamborra, *Phys. Rev. D* **94**, 103009 (2016) [arXiv:1606.09243].
- [20] E. Aprile *et al.* (XENON), *J. Cosmol. Astropart. Phys.* **04** (2016) 027; D.S. Akerib *et al.* (LZ), *Nucl. Inst. Meth. Phys. Res. A* **953**, 163047 (2020) [arXiv:1910.09124]; J. Aalbers *et al.* (DARWIN) *JCAP*

- 11 (2016) 017 [arXiv:1606.07001].
- [21] T.M. Undagoitia and L. Rauch, *J. Phys. G* **43**, 013001 (2016).
- [22] G.V. Domogatskiĭ and G.T. Zatsepin, *Proc. Int. Conf. Cosmic Rays* **2**, 1030 (1965); *ibid* CERN Scientific Report No. **28**, 161 (1969); G.S. Bisnovatyĭ-Kogan and E.F. Seidov, *JETP Lett.* **19**, 319 (1974); D. Cline, E. Fenyves, G. Fuller, B. Meyer, J. Park, and J. Wilson, *Astrophys. Lett. Commun.* **27**, 403 (1990); *Phys. Rev. D* **50**, 720 (1994); G.M. Fuller, W.C. Haxton, and G.C. McLaughlin, *Phys. Rev. D* **59**, 085005 (1999); S. Elliott, *Phys. Rev. C* **62**, 065802 (2000).
- [23] E. Kolbe and K. Langanke, *Phys. Rev. C* **63**, 025802 (2001).
- [24] J. Engel, G. C. McLaughlin, and C. Volpe, *Phys. Rev. D* **67**, 013005 (2003).
- [25] A. Bandyopadhyay, P. Bhattacharjee, S. Chakraborty, K. Kar, and S. Saha, *Phys. Rev. D* **95**, 065022 (2017).
- [26] P. Bhattacharjee and K. Kar, *Eur. Phys. J. Spec. Top.* **230**, 505–515 (2021); <https://doi.org/10.1140/epjs/s11734-021-00002-6>
- [27] E. Aprile et al (XENON) in Ref. [20].
- [28] S. Agostinelli et al, *Nucl. Inst. Meth. Phys. Res., A* **506**, 250 (2003); <https://geant4.web.cern.ch/>
- [29] T. Fischer, S.C. Whitehouse, A. Mezzacappa, F.-K. Thielemann, and M. Liebendörfer, *Astron. Astrophys.* **517**, A80 (2010).
- [30] The 1 kpc distance to the SN is taken for illustration and for easy scaling of our results. The median distance (from earth) of CCSN progenitors in the Milky Way is estimated to be $\simeq 9$ kpc [4] [see also S.M. Adams, C.S. Kochanek, J.F. Beacom, M.R. Vagins, and K.Z. Stanek, *Astrophys. J.* **778**, 164 (2013)], with $\sim 10\%$ (90%) of these lying within 5 (15) kpc.
- [31] M.T. Keil, G.G. Raffelt, and H.T. Janka, *Astrophys. J.* **590**, 971 (2003).
- [32] E. Borriello, S. Chakraborty, A. Mirizzi, P.D. Serpico, and I. Tamborra, *Phys. Rev. D* **86**, 083004 (2012).
- [33] See, e.g., R.N. Mohapatra and P.B. Pal, *Massive Neutrinos in Physics and Astrophysics*, 3rd Ed. (World Scientific, Singapore, 2004).
- [34] H. Duan, G.M. Fuller, and Y.-Z. Qian, *Annu. Rev. Nucl. Part. Sci.* **60**, 569 (2010).
- [35] S. Chakraborty, R. Hansen, I. Izaguirre, and G. Raffelt, *Nucl. Phys. B* **908**, 366 (2016).
- [36] F. Capozzi, B. Dasgupta, A. Mirizzi, M. Sen, and G. Sigl, *Phys. Rev. Lett.* **122**, 091101 (2019).
- [37] S. Chakraborty, T. Fischer, A. Mirizzi, N. Saviano, and R. Tomas, *Phys. Rev. Lett.* **107**, 151101 (2011); *Phys. Rev. D* **84**, 025002 (2011).
- [38] J.D. Lewin and P.F. Smith, *Astropart. Phys.* **6**, 87 (1996).
- [39] T. Kuramoto, M. Fukugita, Y. Kohyama, and K. Kubodera, *Nucl. Phys. A* **512**, 711 (1990).
- [40] G.M. Fuller, W.C. Haxton, and G.C. McLaughlin, *Phys. Rev. D* **59**, 085005 (1999).
- [41] E. Kolbe, K. Langanke and G. Martinez-Pinedo, *Phys. Rev. C* **60**, 052801 (1999).
- [42] W.J. Huang, M. Wang, F.G. Kondev, G. Audi and S. Naimi, *Chinese Phys.* **C45**, 030002 (2021); M. Wang, W.J. Huang, F.G. Kondev, G. Audi and S. Naimi, *Chinese Phys.* **C45**, 030003 (2021); https://www-nds.iaea.org/amdc/ame2020/mass_1.mas20.txt
- [43] J. Engel, *Phys. Rev. C* **57**, 2004 (1998).
- [44] S. Ünlü, H.A. Aygör, N. Çakmak and C. Selam, *Turkish J. Phys.* **40**, 304 (2016).
- [45] O. Moreno, R. Alvarez-Rodriguez, R. Sarriguren, E. Moya de Guerra, J.M. Udias and J.R. Vignote, *Phys. Rev. C* **74**, 054308 (2006).
- [46] M. Beiner, H. Flocard, N. Van Giai, and P. Quentin, *Nucl. Phys. A* **238**, 29 (1975).
- [47] <http://lise.nslc.msu.edu/pace4.html>; O.B. Tarasov and D. Bazin, *Nucl. Instrum. Methods Phys. Res., Sect. B* **204**, 174 (2003).
- [48] A. Gavron, *Phys. Rev. C* **21**, 230 (1980).
- [49] <https://www.nndc.bnl.gov/exfor/endf00.jsp>
- [50] S. Ghosh, A. Bandyopadhyay, P. Bhattacharjee, S. Chakraborty, K. Kar and S. Saha, arXiv:2201.10538.
- [51] https://geant4-userdoc.web.cern.ch/UsersGuides/PhysicsListGuide/html/reference_PL/QGSP_BERT.html#related-physics-lists
- [52] M. Szydagis, N. Barry, K. Kazkaz, J. Mock, D. Stolp, M. Sweany, M. Tripathi, S. Uvarov, N. Walsh, and M. Woods, *J. Instrum.* **6**, P10002 (2011).
- [53] M. Szydagis, A. Fyhrie, D. Thorngren, and M. Tripathi, *J. Instrum.* **8**, C10003 (2013).
- [54] B. Lenardo, K. Kazkaz, A. Manalaysay, J. Mock, M. Szydagis, and M. Tripathi, *IEEE Trans. Nucl. Sci.* **62**, 3387 (2015).
- [55] D. S. Akerib et al [LUX], *Phys. Rev. Lett.* **116**, 161301 (2016) [arXiv:1512.03506].
- [56] <https://nest.physics.ucdavis.edu/>
- [57] S. Ghosh et al (2022), in preparation.
- [58] E. Aprile and T. Doke, *Rev. Mod. Phys.* **82**, 2053 (2010) [arXiv:0910.4956].
- [59] E. Aprile et al (XENON collaboration), *Phys. Rev. Lett.* **123**, 251801 (2019).
- [60] <https://physics.nist.gov/PhysRefData/Star/Text/ESTAR.html>
- [61] E. Aprile et al (XENON collaboration), *Phys. Rev. D* **99**, 112009 (2019) [arXiv:1902.11297].
- [62] E. Aprile et al [XENON], *JCAP* **11**, 031 (2020) [arXiv:2007.08796].
- [63] S. Gardiner, *Computer Phys. Communications* **269**, 108123 (2021).